ANALYZE 2-D HEAT TRANSFER OF ULTRAFAST LASER HEATED THIN FILMS UNDER SIZE EFFECTS

by

Yudong MAO [a*], ***Guochen ZHAO*** [a], ***Mingzhi YU*** [a], ***Xianzheng WANG*** [a], ***Jin LI*** [b], ***Kaimin YANG*** [a], ***and Shouyu LIU*** [a]

[a] School of Thermal Engineering, Shandong Jianzhu University, Jinan, China
[b] School of Sciences, Shandong Jianzhu University, Jinan, China

Original scientific paper
https://doi.org/10.2298/TSCI220819043M

An improved dual-phase-lagging model which reflects size effects caused by nanostructures is utilized to investigate the 2-D thermal conduction of nanosilicon films irradiated by ultrafast laser. The integral transformation method is used to solve the conduction governing equation based on the improved dual-phase-lagging model. The variation of the internal temperature along the thickness direction and the radial direction of the thin film is analyzed. We find that the temperature increases rapidly in the heated region of the film, and as time goes by, the energy travels from the heated end to another end in a form of wave. Although both the improved dual-phase-lagging model and the dual-phase-lagging model can obtain similar thermal wave temperature fields, the temperature distribution in the film obtained by the improved dual-phase-lagging model is relatively flat, especially for high Knudsen number. Under the same Knudsen number, the temperature obtained by the 2-D improved dual-phase-lagging model is higher than that obtained by the 1-D model, and the temperature difference becomes larger and larger as time elapses.

Key words*: ultrafast laser heating, size effects, dual-phase-lagging model, integral transformation method*

Introduction

Ultrafast laser heating technology has the characteristics of high energy density, low ablation threshold*, etc.*, it is widely used in thermal processing [1-3], information storage [4, 5], nanofilm preparation [6], and other fields [7]. The ultrafast laser heating technology has the characteristic of high precision, which makes it have an important position in medical fields [8], such as the production of fine medical equipment and fine medical operations. Due to its extremely short thermal action time and extremely high peak power, it often produces large temperature gradients in the thermal zone [9, 10]. Study the heat transfer phenomenon of ultrafast laser heating technology has become more and more important.

The classical Fourier's law is a basic law describing the law of macroscopic heat conduction, but it can not accurately describe the heat transfer mechanism in an ultra-short time. Cattaneo [11] and Vernotte [12] proposed a CV heat conduction model based on Fourier's law, and the relaxation time of the heat flow vector is used in it. Although the CV model can show some phenomena of ultra-fast heat transfer [13], it still not preciseness enough. Tzou [14] pro-

[*] Corresponding author, e-mail: maoyudong@sdjzu.edu.cn

posed a dual-phase-lagging (DPL) model which takes not only the relaxation time of heat flow vector but also the relaxation time of temperature gradient into account. This model can accurately describe the mechanism of ultrafast heat transfer [15, 16]. In recent years, as a new type of nanomaterials, nanofilm has received extensive attention [17-19]. The ultra-small structure size and extraordinary physical properties make it have unique advantages in the fields of photonics, thermodynamics [20], medicine, energy devices [21], *etc*. Therefore, it has important theoretical value to study the heat transfer mechanism of ultrafast laser in ultra-short time and at ultra-small size for the preparation, thermal processing and phase transformation of films. However, the size effect caused by the ultra-small size complicates the thermal conductivity of nanofilms. The size effect of thin film refers to the effect of sudden change of properties when the thickness of thin film decreases to a certain degree, and the thermal conductivity of thin film will drop sharply with the decrease of thickness. Based on the extended irreversible thermodynamic theory, a non-Fourier model reflecting memory and non-local effects was developed by Alvarez and Jou [22-25], and the effective thermal conductivity of the response size effect and related hysteresis parameters were proposed.

In this paper, an improved DPL heat conduction model reflecting the size effect is used to study the heat transfer problem of ultrafast laser heating of nanofilms, and the integral transformation method is used to solve the control equations. In this article, you can see how size effects affect the energy transfer of laser-heated thin films. It has important theoretical significance for the thermal conductivity of nanofilms heated by ultrafast lasers.

Theoretical analysis

Improved DPL thermal conduction model

The DPL model proposed by Tzou [14] is shown:

$$q\left(r,t+\tau_q\right)=-\lambda_0\nabla T\left(r,t+\tau_T\right) \tag{1}$$

where r is the position vector, t – the time variable, q – the heat flux, λ_0 – the thermal conductivity of the material, ∇T – the temperature gradient, τ_q – the lagging time of the heat flow vector q, and τ_T – the lagging time of the temperature gradient ∇T. The effective thermal conductivity proposed by [22-25] can be expressed:

$$\lambda(L)=\frac{\lambda_0}{2\pi^2 Kn^2}\left[\sqrt{1+4(\pi\mathrm{Kn})^2}-1\right]$$

the effective lagging time

$$\tau_e=\frac{1}{4}\tau_q$$

After considering the memory and size effects, the DPL model is improved:

$$q\left(r,t+\tau_e\right)=-\lambda(L)\nabla T\left(r,t+\tau_T\right) \tag{2}$$

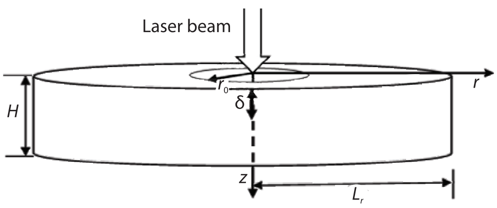

Figure 1. Physical model/schematic diagram of ultrafast laser irradiation of silicon thin film

Mathematical derivation

The physical model of the laser irradiated on the surface of the silicon film is shown in fig. 1 [26], where r_0 is the laser spot radius, δ is the longitudinal penetration depth of the laser, H is the thickness of the film, and Kn = l/H where l is the mean free path of hot carriers and L_r is the radius of the film, L_r = 750 nm. The ultrafast laser irradiates the nanosilicon film vertically from the center of the film, and the contact surface between the film and the outside is a heat-insulating surface.

Combined with the energy conservation equation, the governing equation is obtained on the improved DPL model:

$$\lambda(L)\left(\begin{array}{l}\dfrac{\partial^2 T(r,z,t)}{\partial r^2}+\dfrac{1}{r}\dfrac{\partial T(r,z,t)}{\partial r}+\dfrac{\partial^2 T(r,z,t)}{\partial z^2}+\\ +\tau_T\left(\dfrac{\partial^3 T(r,z,t)}{\partial r^2\partial t}+\dfrac{1}{r}\dfrac{\partial T(r,z,t)}{\partial r\partial t}+\dfrac{\partial^3 T(r,z,t)}{\partial z^2\partial t}\right)\end{array}\right)+$$
$$+S(r,z,t)+\frac{1}{4\tau_q}\frac{S(r,z,t)}{\partial t}=C_v\frac{\partial T(r,z,t)}{\partial t}+C_v\frac{1}{4}\tau_q\frac{\partial^2 T(r,z,t)}{\partial t^2} \tag{3}$$

where C_v is the specific heat capacity of constant volume, relaxation time $\tau_q = \ell/v$, v is the average group velocity of hot carriers, and S – the energy absorption density of the laser [9, 10]:

$$S(r,z,t)=0.94J\frac{1-R}{t_p\delta}\exp\left(-\frac{z}{\delta}-\frac{r^2}{r_0^2}-1.992\frac{t}{t_p}\right) \tag{4}$$

where J is the laser energy density, R – the surface reflectivity, r_0 – the laser spot radius, δ – the laser penetration depth, and t_p – the continuous heating time of the laser, the boundary and initial conditions are expressed:

$$\frac{\partial T(r,z,t)}{\partial z}/_{z=0}=0,\quad \frac{\partial T(r,z,t)}{\partial z}/_{z=H}=0,\quad \frac{\partial T(r,z,t)}{\partial r}/_{r=L_r}=0 \tag{5}$$

$$T(r,z,t)/_{t=0}=T_0,\quad \frac{\partial T(r,z,t)}{\partial t}/_{t=0}=\frac{S(r,z,t)}{C_v} \tag{6}$$

Introduce the dimensionless parameters:

$$z^*=\frac{z}{H},\quad r^*=\frac{r}{L_r},\quad T^*=\frac{T-T_0}{T_0},\quad t^*=\frac{t}{t_p} \tag{7}$$

Arranged as dimensionless governing equation:

$$\frac{1}{4}a\frac{\partial^2 T^*(r^*,z^*,t^*)}{\partial t^{*2}}+\frac{\partial T^*(r^*,z^*,t^*)}{\partial t^*}=$$
$$=Dt_p\left(\begin{array}{l}\dfrac{1}{L_r^2}\left(\dfrac{\partial^2 T(r^*,z^*,t^*)}{\partial r^{*2}}+\dfrac{1}{r^*}\dfrac{\partial T(r^*,z^*,t^*)}{\partial r^*}\right)+\dfrac{1}{H^2}\dfrac{\partial^2 T(r^*,z^*,t^*)}{\partial z^{*2}}+\\ +ab\left(\dfrac{1}{L_r^2 t_p}\left(\dfrac{\partial^2 T(r^*,z^*,t^*)}{\partial r^{*2}}+\dfrac{1}{r^*}\dfrac{\partial T(r^*,z^*,t^*)}{\partial r^*}\right)+\dfrac{1}{H^2 t_p}\dfrac{\partial^3 T(r^*,z^*,t^*)}{\partial z^{*2}\partial t^*}\right)\end{array}\right)+$$
$$+(1-0.498a)S_0 Q^*(r^*,z^*,t^*) \tag{8}$$

$$Q(r^*,z^*,t^*)=\exp\left(-\zeta z^*-\varepsilon^{*2}r^{*2}-1.992t^*\right) \tag{9}$$

$$S_0 = 0.94J\frac{1-R}{T_0 C_v \delta},\ \xi = \frac{H}{\delta},\ \varepsilon = \frac{L_r}{r},\ a = \frac{\tau_q}{t_p},\ b = \frac{\tau_T}{\tau_q} \tag{10}$$

In eq. (8), the ξ, ε, a, and b are intermediate parameters with no special meaning.
The boundary and initial conditions are shown:

$$\frac{\partial T^*\left(r^*,z^*,t^*\right)}{\partial z^*}/_{z^*=0} = 0,\ \frac{\partial T^*\left(r^*,z^*,t^*\right)}{\partial z^*}/_{z^*=1} = 0,\ \frac{\partial T^*\left(r^*,z^*,t^*\right)}{\partial r^*}/_{r^*=1} = 0 \tag{11}$$

$$T^*\left(r^*,z^*,t^*\right)/_{t^*=0} = 0,\ \frac{\partial T^*\left(r^*,z^*,t^*\right)}{\partial t^*}/_{t^*=0} = S_0 Q^*\left(r^*,z^*,t^*\right) \tag{12}$$

Solve eqs. (8)-(12) using integral transformation method, first perform integral transformation on r^*. Equation (13) is the inverse integral transformation on r^*, and eq. (14) is the positive integral transformation on r^*:

$$T^*\left(r^*,z^*,t^*\right) = \sum_{m=0}^{\infty}\frac{J_0\left(\beta_m r^*\right)}{N\left(\beta_m\right)}\overline{T}\left(\beta_m,z^*,t^*\right) \tag{13}$$

$$\overline{T}\left(\beta_m,z^*,t^*\right) = \int_0^1 r^* J_0\left(\beta_m,r^*\right)T\left(r^*,z^*,t^*\right)\mathrm{d}r^* \tag{14}$$

where $J_0(\beta_m r^*)$ is the 0th order Bessel function of the first kind [27-29], solution for$J_1(\beta_m r^*) = 0$ is β_m, $\beta_m \geq 0$, $m = 1, 2, 3...$, $N(\beta_m) = 1/2J_0^2(\beta_m)$.When $m = 0$, $\beta_m = 0$, $N(\beta_0) = 1/2$.

Then perform an integral transformation on z^*, eq. (15) is the inverse integral transformation on z^*, and eq. (16) is the positive integral transformation on z^*:

$$\overline{T}^*\left(\beta_m,z^*,t^*\right) = \sum_{n=1}^{\infty}\frac{Z\left(\eta_n z^*\right)}{N\left(\eta_n\right)}\overline{\overline{T}}^*\left(\beta_m,\eta_n,t^*\right) \tag{15}$$

$$\overline{\overline{T}}^*\left(\beta_m,\eta_n,t^*\right) = \int_0^1 Z^*\left(\eta_n,z^*\right)\overline{T}^*\left(\beta_m,z^*,t^*\right)$$

$$\eta_n = n\pi,\ n = 0,1,2,3...N\left(\eta_n\right) = \begin{cases}\frac{1}{2},\eta_n \neq 0\\ 1,\eta_n = 0\end{cases} \tag{16}$$

After sorting out, the original dimensionless governing equation is written:

$$\frac{1}{4}a\frac{\partial^2\overline{\overline{T}}^*\left(\beta_m,\eta_n,t^*\right)}{\partial t^{*2}} + \left(1+ab\gamma_{mn}\right)\frac{\partial\overline{\overline{T}}^*\left(\beta_m,\eta_n,t^*\right)}{\partial t^*} + \gamma_{mn}\overline{\overline{T}}^*\left(\beta_m,\eta_n,t^*\right) = = \left(1-0.498a\right)S_0\overline{\overline{Q}}^*\left(\beta_m,\eta_n,t^*\right) \tag{17}$$

$$\gamma_{mn} = \left(\frac{\beta_m^2}{L_r^2} + \frac{\eta_n^2}{H^2}\right)Dt_p \tag{18}$$

$$\overline{\overline{Q}}^*\left(\beta_m,\eta_n,t^*\right) = \int_0^1\int_0^1 r^* J_0\left(\beta_m r^*\right)\exp\left(-\varepsilon^{*2}r^{*2}\right)\cos\left(\eta_n z^*\right)\exp\left(-\zeta z^* - 1.992t^*\right)\mathrm{d}r^*\mathrm{d}z^* \tag{19}$$

$$\overline{\overline{T}}^*\left(\beta_m,\eta_n,t^*\right)_{/i=0}=0,\ \frac{\overline{\overline{T}}^*\left(\beta_m,\eta_n,t^*\right)}{\partial t^*}{}_{/i=0}=S0\overline{\overline{Q}}^*\left(\beta_m,\eta_n,t^*\right) \tag{20}$$

Equation (17) is a second-order non-homogeneous linear ODE, solve the expression of the dimensionless temperature after the positive integral transformation:

$$T^*\left(r^*,z^*,t^*\right)=\sum_{m=0}^{\infty}\sum_{n=0}^{\infty}\frac{J_0\left(\beta_m r^*\right)\cos\left(\eta_n z^*\right)}{N\left(\beta_m\right)N\left(\eta_n\right)}\cdot \\ \cdot\left[C_1F_1\left(\beta_m,\eta_n,t^*\right)+C_2F_2\left(\beta_m,\eta_n,t^*\right)+C\exp\left(-1.992t^*\right)\right] \tag{21}$$

make $\Delta = (1 + ab\gamma_{mn})2 - a\gamma_{mn}$, the function and parameters in eq. (21) can be expressed:

$$C=\frac{\left(1-0.498a\right)S_0\int\limits_0^1 r^*J_0\left(\beta_m r^*\right)\exp\left(-\zeta z^*\right)\mathrm{d}r^*\int\limits_0^1\cos\left(\eta_n z^*\right)\exp\left(-\varepsilon^{*2}r^{*2}\right)\mathrm{d}z^*}{\left[1.992^2a-1.992\left(1+ab\gamma_{mn}\right)+\gamma_{mn}\right]} \tag{22}$$

– when $\Delta > 0$

$$F_1\left(\beta_m,\eta_n,t^*\right)=\mathrm{e}^{\frac{-\left(1+ab\gamma_{mn}\right)+\sqrt{\Delta}}{2a}},\ F_2\left(\beta_m,\eta_n,t^*\right)=\mathrm{e}^{\frac{-\left(1+ab\gamma_{mn}\right)-\sqrt{\Delta}}{2a}} \tag{23}$$

– when $\Delta = 0$

$$F_1\left(\beta_m,\eta_n,t^*\right)=\mathrm{e}^{\frac{-\left(1+ab\gamma_{mn}\right)}{2a}t^*},\ F_2\left(\beta_m,\eta_n,t^*\right)=\mathrm{e}^{\frac{-\left(1+ab\gamma_{mn}\right)}{2a}t^*} \tag{24}$$

– when $\Delta < 0$

$$F_1\left(\beta_m,\eta_n,t^*\right)=\mathrm{e}^{\frac{-\left(1+ab\gamma_{mn}\right)}{2a}t^*}\cos\left(\frac{-\sqrt{\Delta}}{2a}\right),\ F_2\left(\beta_m,\eta_n,t^*\right)=\mathrm{e}^{\frac{-\left(1+ab\gamma_{mn}\right)}{2a}t^*}\sin\left(\frac{-\sqrt{\Delta}}{2a}\right) \tag{25}$$

$$C_1=\frac{-C\dfrac{\partial F_2\left(\beta_m,\eta_n,t^*\right)}{\partial t^*}\text{-}\left(1.992C+S_0\int\limits_0^1\begin{matrix}\cos\left(\eta_n z^*\right)\exp\left(-\zeta z^*\right)\mathrm{d}r^*\\ \int\limits_0^1 r^*J_0\left(\beta_m r^*\right)\exp\left(-\varepsilon^{*2}r^{*2}\right)\mathrm{d}z^*\end{matrix}\right)F_2\left(\beta_m,\eta_n,t^*\right)}{F_1\left(\beta_m,\eta_n,t^*\right)\dfrac{\partial F_2\left(\beta_m,\eta_n,t^*\right)}{\partial t^*}-F_2\left(\beta_m,\eta_n,t^*\right)\dfrac{\partial F_1\left(\beta_m,\eta_n,t^*\right)}{\partial t^*}} \\ C_2=\frac{C\dfrac{\partial F_1\left(\beta_m,\eta_n,t^*\right)}{\partial t^*}+\left(1.992C+S_0\int\limits_0^1\begin{matrix}\cos\left(\eta_n z^*\right)\exp\left(-\zeta z^*\right)\mathrm{d}r^*\\ \int\limits_0^1 r^*J_0\left(\beta_m r^*\right)\exp\left(-\varepsilon^{*2}r^{*2}\right)\mathrm{d}z^*\end{matrix}\right)F_1\left(\beta_m,\eta_n,t^*\right)}{F_1\left(\beta_m,\eta_n,t^*\right)\dfrac{\partial F_2\left(\beta_m,\eta_n,t^*\right)}{\partial t^*}-F_2\left(\beta_m,\eta_n,t^*\right)\dfrac{\partial F_1\left(\beta_m,\eta_n,t^*\right)}{\partial t^*}} \tag{26}$$

Apply eqs. (13) and (11) to eq. (19) in turn to do the inverse integral transformation, and finally obtain the solution of the dimensionless temperature in the dimensionless governing eqs. (8)-(10):

$$T^* = \sum_{m=0}^{\infty}\sum_{n=0}^{\infty}\frac{J_0\left(\beta_m r^*\right)\cos\left(\eta_n z^*\right)}{N\left(\beta_m\right)N\left(\eta_n\right)}\left[C_1F_1\left(\beta_m,\eta_n,t^*\right)+C_2F_2\left(\beta_m,\eta_n,t^*\right)+C\exp\left(-1.992t^*\right)\right] \quad (27)$$

If the thermal conductivity λ is equal to λ_0, the heat flux relaxation time is equal to τ_q, the result of the aforementioned equation is the result of describing the problem based on the DPL model.

Results and discussion

Tables 1 and 2 show the physical parameters of silicon thin film and ultrafast laser [30]. The calculation parameters in the table are used for the following calculation results.

Table 1. Thermophysical and geometric parameters of silicon film

Name	Specific heat capacity, C_v [Jm^{-3}K^{-1}]	Thermal conductivity, λ_0 [Wm^{-1}K^{-1}]	The initial temperature, T_0 [K]	Mean free path of hot carriers, l [nm]
Value	$2.3 \cdot 10^6$	148	300	41

Table 2. Ultrafast laser parameters

Name	Laser pulse duration, t_p [Ps]	Laser energy density, J [Jm^{-2}]	Laser penetration depth, δ [nm]	Surface reflectance, R
Value	0.65	732	15.3	0.93

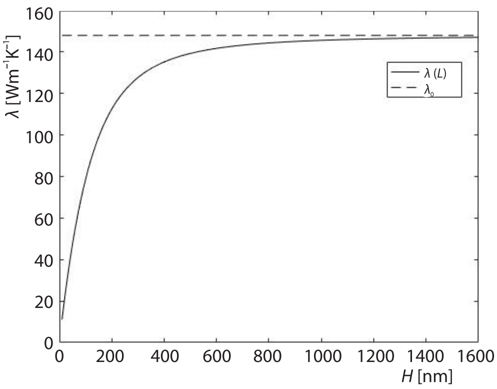

Figure 2. Variation of effective thermal conductivity of silicon film with film thickness

In order to verify the correctness of the expression of $\lambda(L)$, we compare the effective thermal conductivity $\lambda(L)$ of silicon thin film with the thermal conductivity λ_0 of bulk silicon. Figure 2 shows when the thickness of the film is below 100 nm, the effective thermal conductivity increases rapidly with the increase of the thickness, and the rate of increase of the effective thermal conductivity slows down as the thickness continues to increase, and finally gradually approaches the thermal conductivity of bulk silicon. When the film thickness is 410 nm, the effective thermal conductivity is 135.84 W/mK, and when the film thickness is 41 nm, the effective thermal conductivity is only 40.24 W/mK, which shows that the thermal conductivity of the nanofilm at this time is It is greatly affected by the size of the film.

The heat conduction problem of nanosilicon film heated by ultrafast laser based on the improved DPL model is analyzed. Figure 3 shows the temperature distribution map of the film center position along the thickness direction at different time, t^*. Where $b = 0.2$, $b = \tau_t/\tau_q$. It can be seen when the laser is irradiated to the film, the temperature at the center of the heated surface rises rapidly. The temperature of the film increases first and then decreases over time, this is because the laser continues to heat the film before $t^* = 1$, so that the temperature of the film continues to rise, but after $t^* = 1$, the laser no longer heats the film, and the heat is continuously transferred to the interior, causing the temperature to drop. The thickness of the film affected by the laser heat source increases. The amplitude of the temperature rise gradually

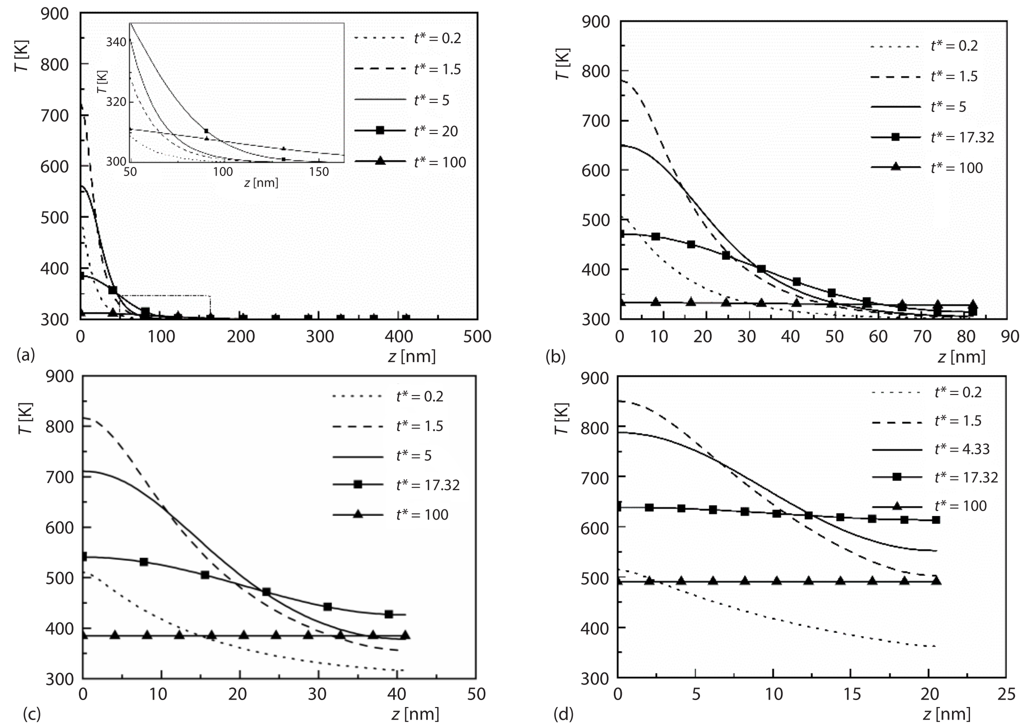

Figure 3. The temperature distribution diagram of the center position of the thin film along the thickness direction of the improved DPL model at different time t^*; (a) Kn = 0.1, H = 410 nm, (b) Kn = 0.5, H = 82 nm, (c) Kn = 1, H = 41 nm, and (d) Kn = 2, H = 20.5 nm

slows down along the thickness direction, and finally it reaches a steady-state. This is because in the thin layer near the surface of the silicon film, the temperature rise mainly comes from the irradiation of the laser light source. As the depth increases, the absorption of laser irradiation decreases, and the heat conduction in the film occupies the main position at this moment. As the depth of the film increases further, the energy generated by absorbing the laser heat source can be ignored, and the temperature rise inside the film is completely controlled by heat conduction.

It can be found by observing figs. 3(a)-3(d). When $t^* = 100$, the temperature of the thin film with Kn = 0.1 has not reached a stable state along the thickness direction. Although the temperature of the film with Kn = 0.5 does not reach a completely stable state along the thickness direction, the variation range of the temperature along the thickness direction is smaller than that when Kn = 0.1. When $t^* = 100$, the temperature of the film with Kn = 1 has reached a stable state along the thickness direction, which is about 384.94 K. The film with Kn = 2 is along the thickness direction the temperature is about 491.22 K. It can be concluded that with the increase of Knudsen number, the time required for the temperature in the film to reach a stable state becomes shorter. It is also found from the figure that at the same time, the temperature at the center of the heated surface of the film increases with the increase of Knudsen number, and the temperature maintained inside the film in the steady-state increases with the increase of Knudsen number. This is because with the increase of Knudsen number, the film thickness decreases and the thermal conductivity becomes smaller, which reduces the energy received inside the film. In addition, the adiabatic boundary condition selected in this paper also causes the temperature at the center of the heated surface of the film to rise with the increase of Knudsen number. At the same time, the shortening of the film thickness will cause the energy absorbed per unit thickness to increase, so the temperature of the film along the thickness direction increases with Knudsen number in the steady-state.

There is no temperature *bump* phenomenon in the improved DPL results. Although the improved DPL considers the hysteresis effect of the heat flow vector and temperature gradient, the thermal conductivity of the film is far from the macroscopic thermal conductivity due to the consideration of the size effect of the film at the same time, resulting in insufficient accumulation of energy inside the film to make the temperature at the next point It is higher than the previous one, but it is worth noting that the heat inside the film is still propagated in the form of waves.

Figure 4 shows the temperature distribution along the radial direction at the center of the heated surface of the film at different times t^*. Where $b = 0.2$, and the radial size of the film remains unchanged. It can be seen from the figure that the temperature at the center of the heated surface of the film increases rapidly with time and then decreases, and the radial size affected by energy disturbance also increases gradually. These phenomena are consistent with the thickness direction in qualitative analysis. It is worth noting that the size range of energy sweep along the radial direction of the internal temperature of the film is smaller than that in the thickness direction at the same time. This phenomenon is not difficult to explain. As can be seen from the expression of laser energy density, the energy carried by the laser in the radial direction is far less than that in the thickness direction, so the energy accumulated along the

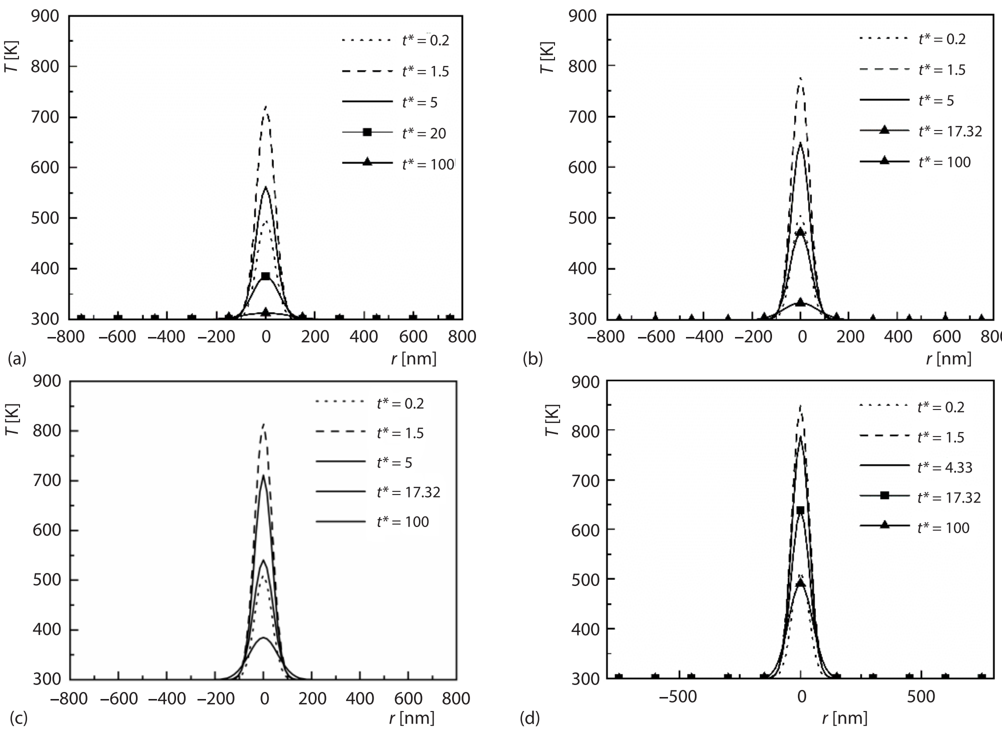

Figure 4. The radial temperature distribution diagram of the central position of the thin film at different time t^* of improved DPL; (a) Kn = 0.1, H = 410 nm, (b) Kn = 0.5, H = 82 nm, (c) Kn = 1, H = 41 nm, (d) Kn = 2, H = 20.5 nm

radial unit length of the film is far less than that in the thickness direction. It causes the fluctuation of heat in the radial direction be less than that in the thickness direction. As can be seen from figs. 4(a)-4(d), with the increase of Knudsen number, the temperature at the center of the heated surface of the film increases, and at the same time, the internal radial temperature also increases. This is because with the shortening of the thickness size, the heat absorbed per unit volume of the film increases with the increase of the heat per unit thickness size. Figure 4 also shows that as time goes on, even though the radial size affected by the laser heat gradually increases, it does not transfer to the radial edge of the film. This is caused by two reasons. One is that the energy carried by the laser in the radial direction is low, so the heat wave has reached a stable state before reaching the radial edge. The second reason is that the radial size is 750 nm, which is larger than the thickness direction, so the thermal wave effect displayed is not obvious compared with the thickness.

Figure 5 shows the effect of the temperature gradient hysteresis time based on the improved DPL heat conduction model on the internal heat conduction process of the film. Figure 5(a) shows the temperature distribution of the film at different b when Kn = 0.1 and $t^* = 10$. It can be seen from the figure that the temperature distribution of the film changes more slowly with the increase of b. This is because with the increase of b, the lag time of temperature gradient in the film increases. When $b = 0$, the temperature near the surface of the film is basically the same as the temperature at the surface of the film, then it drops rapidly. This is because the temperature hysteresis effect inside the film is not considered when $b = 0$, resulting in more energy accumulation inside the film. This phenomenon also explains that heat is transferred in the form of *wave* in the improved DPL heat conduction model. Figure 5(b) shows the film temperature distribution with different b when Kn = 0.5 and $t^* = 10$. It can be seen from fig. 5(b) that the temperature near the film surface drops slowly when $b = 0$, and then decreases rapidly with the increase of depth, and the film temperature changes more gently with the increase of b. We can get a conclusion: If the lag time of the temperature gradient in the film is larger, the temperature distribution inside the film is smoother and the time required to reach a stable state is shorter.

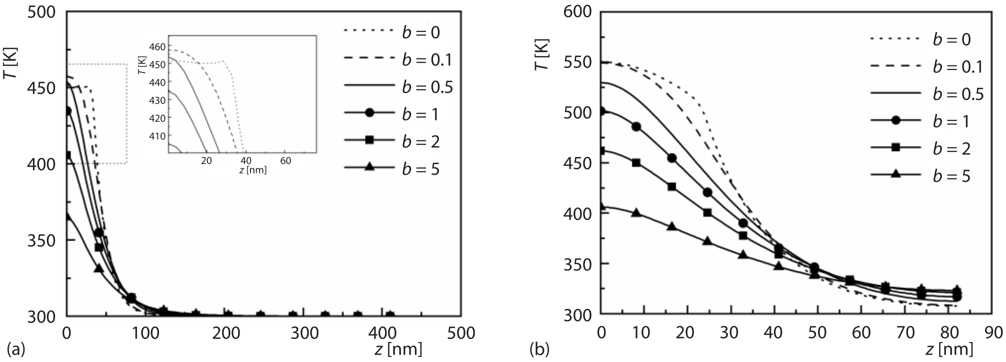

Figure 5. Temperature distributions of thin films along the thickness direction at different b values at $t^* = 10$; (a) Kn = 0.1, H = 410 nm and (b) Kn = 0.5, H = 82 nm

In order to show the influence of the size effect on the thermal wave in the film, the improved DPL (imp) result when $b = 0.2$ is selected here for comparison with the DPL result, as shown in fig. 6. The temperature peak of the film in the improved DPL results always exists in the center of the heated surface, while the temperature peak in the DPL results will appear inside the film. This is because the thermal conductivity of the film in the DPL is greater than that of the improved DPL, the energy received inside the film is more than that of the improved DPL. Due to the hysteresis effect of the heat vector, a *bump* in temperature occurs when energy builds up at a point that makes the temperature higher than the previous point. In the initial heating stage, the temperature at the center of the heated surface of the film simulated by DPL is higher than that of the improved DPL. With the increase of heating time, the temperature of the improved DPL is gradually higher than that of the DPL. The time when the improved DPL is higher than that of the DPL is more and more earlier with the increase of Knudsen number. When Kn = 2 and t^* = 0.2, the temperature at the center of the heated surface is higher than that in the DPL model. Observing fig. 6(a)-6(d), we can also find that it takes a shorter time to reach a stable state based on the improved DPL model. This is because the size effect of the nanofilm is used in the improved DPL thermal conductivity model, resulting in a low internal thermal conductivity of the film. The internal temperature of the film is always lower than the temperature at the center of the film surface before reaching the stable state, and gradually decreases along the thickness (radius) of the film. It saves the time required for the reciprocating cycle of the internal temperature of the film in the DPL model from *low to high and then low*. In summary, the size effect in the structure of the nanofilm makes the internal thermal conduction process of the film more complex, and the influence on the internal thermal conductivity of the film is also not negligible.

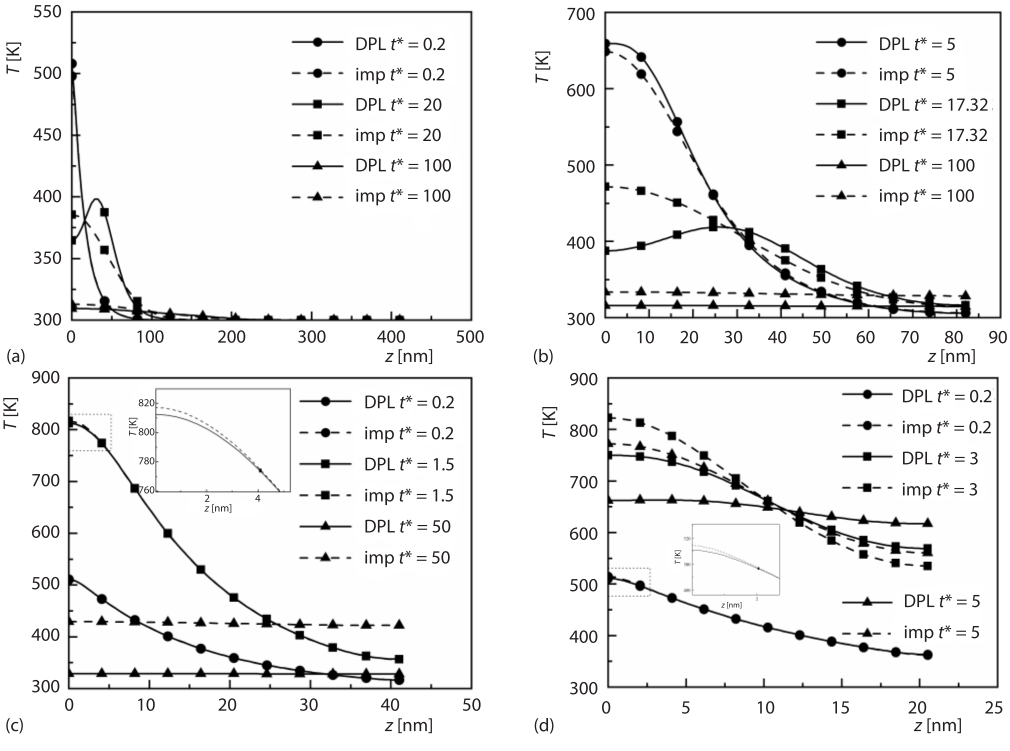

Figure 6. Improved DPL and DPL results; (a) Kn = 0.1, H = 410 nm, (b) Kn = 0.5, H = 82 nm, (c) Kn = 1, H = 41 nm, and (d) Kn = 2, H = 20.5 nm

Figure 7 shows the temperature distribution of 1-D and 2-D DPL in the thickness direction. The 2-D result of temperature in thickness direction is lower than that in 1-D at the same time, and the temperature difference becomes larger and larger as time elapses. This is because the 2-D thermal conductivity model takes the radial dimension of the film into account.

The energy carried by the laser in the radial direction is less than that in the thickness irection, resulting in the energy transferred in the thickness direction the radial direction, and the energy is transferred more and more over time. Therefore, if the radial dimension of the film is considered, the calculation results of the internal temperature of the film will be greatly affected.

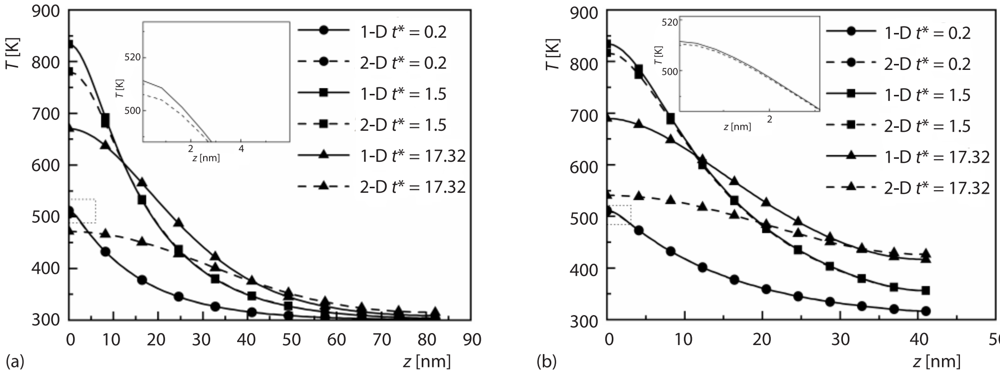

Figure 7. Comparison analysis diagram of 1-D and 2-D improved DPL results; (a) Kn =0.5, *H* = 82 nm and (b) Kn=1, *H* = 82 nm

Conclusion

In this paper, the integral transformation method is used to study the heat conduction problem of ultra-fast laser heating nanosilicon film based on an improved DPL model which reflects size effects. The results show that the temperature in the film increases first and then decreases with time. In the thin layer near the surface of the silicon film, the temperature rise is mainly caused by the irradiation of the laser source. The heat conduction in the depth direction of the film gradually occupies a dominant position. The longer the temperature gradient lag time in the film, the less time it takes for the temperature inside the film to reach a steady-state. By comparing the results of the improved DPL and DPL, the temperature distribution in the film obtained by the improved DPL model is relatively flat after considering the size effect inside the film, and the peak temperature of the film is always located in the center of the film. The size effect in the nanostructure has an important influence on the thermal conductivity process inside the film. The temperature in the thickness direction of the 2-D model is lower than that in the 1-D model, so the radial dimension of the film can't be ignored when studying the thermal conductivity of the laser heated nanofilms.

Acknowledgment

The supports of our research by Jinan Scientific research leader Studio (2019GXRC066) and Project of Shandong Province Higher Educational Science and Technology Program (J16LG07) are greatly appreciated.

Nomenclature

C_v – specific heat capacity, [Jm^{-3}K^{-1}]
J – laser energy density, [Jm^{-2}]
l – mean free path of hot carriers, [nm]
R – surface reflectance, [–]
T_0 – initial temperature, [K]
t_p – laser pulse duration, [ps]

Greek symbols

δ – laser penetration depth, [nm]
λ_0 – thermal conductivity, [Wm^{-1}K^{-1}]
v – average group velocity of hot carriers, [nmps^{-1}]

Reference

[1] Guo, H., *et al*., Patterned Graphene Oxide by Spatially-Shaped Femtosecond Laser (in Chinese), *Chinese Journal of Lasers*, *48* (2021), 2, pp. 292-300
[2] Li, Y. L., *et al.*, Patterning of Graphene by Light Field Modulated Nanosecond Laser (in Chinese), *High Power Laser and Particle Beams*, *30* (2018), 12, pp. 148-151
[3] Ehsan, K. D., *et al.*, Numerical Study of 3-D Microscale Heat Transfer of a Thin Diamond Slab under Fix and Moving Laser Heating, *Thermal Science*, *23* (2019), 5B, pp. 3035-3045
[4] Ghai, S. S., *et al*., A Novel Heat Transfer Model and Its Application Information Storage Systems, *Journal of Applied Physics*, *97* (2005), 10, pp. 1-3
[5] Li, F. J., Coherent Synthesis of Ultrashort Pulse Fiber Laser Based on Balanced Difference Method, *Thermal Science*, *21* (2021), 6A, pp. 4027-4034
[6] Mo, G. K., *et al*., Preparation of Low-Resistivity GZO Thin Films Using Pulsed Laser Deposition and Investigation of Optoelectronic Properties (in Chinese), *Chinese Journal of Lasers*, *46* (2019), 10, pp. 204-210
[7] Nenad, D. M., Application of the Laser Pulse Method of Measuring Thermal Diffusivity to Thin Alumina Silicon Samples in a Wide Temperature Range, *Thermal Science*, *14* (2014), 2, pp. 417-423
[8] Wang, C. D., *et al*., Powder Separation and Its Suppression during Laser Cladding of Medical Ti/HA (in Chinese), *Chinese Journal of Lasers*, *47* (2020), 12, pp. 57-68
[9] Tzou, D. Y., Chiu, K. S., Temperature-Dependent Thermal Lagging in Ultrafast Laser Heating, *International Journal of Heat and Mass Transfer*, *44* (2001), 9, pp. 1725-1732
[10] Tzou, D. Y., et al., Hot-Electron Blast Induced by Ultrashort-Pulsed Lasers in Layered Media, *International Journal of Heat and Mass Transfer*, *45* (2002), 16, pp. 3369-3382
[11] Cattaneo, C., A form of Heat Conduction Equation Which Eliminates the Paradox of Instantaneous Propagation, *Compte- Rendus*, *247* (1958), pp. 431-435
[12] Vernotte, P., Some Possible Complications in the Phenomena of Thermal Conduction, *Compte-Rendus*, *252* (1961), pp. 2190-2193
[13] Guo, S. L., *et al*., Effects of Non-Fourier Heat Conduction and Surface Heating Rate on Thermoelastic Waves in Semi-Infinite Ceramics Subject to Thermal Shock, *Ceramics International*, *47* (2021), 12, pp. 17494-17501
[14] Tzou, D. Y., The Generalized Lagging Response in Small-Scale and High-Rate Heating, *International Journal of Heat and Mass Transfer*, *38* (1995), 17, pp. 3231-3234
[15] Wang, L., Xu, M., Well-Posedness and Solution Structure of Dual-Phase-Lagging Heat Conduction, *International Journal of Heat and Mass Transfer*, *48* (2005), 9, pp. 1165-1171
[16] Xu, M., Wang, L., Thermal Oscillation and Resonance in Dual-Phase-Lagging Heat Conduction, *International Journal of Heat and Mass Transfer*, *45* (2002), 5, pp. 1055-1061
[17] Joshi, A. A., Majumdar, A., Transient Ballistic and Diffusive Phonon-Heat Transport in Thin Films, *Journal of Applied Physics*, *74* (1993), 1, pp. 31-39
[18] Torii, S. C., Yang, W. J., Heat Transfer Mechanisms in Thin Film With Laser Heat Source, *International Journal of Heat and Mass Transfer*, *48* (2005), 3-4, pp. 537-544
[19] Hua, Y. C., Cao, B. Y., Phonon-Ballistic-Diffusive Heat Conduction in Silicon Nanofilms by Monte-Carlo simulations, *International Journal of Heat and Mass Transfer*, *78* (2014), Nov., pp. 755-759
[20] Peng, Y., Yan, Z., Characterization of Laser-Induced Local Heating in a Substrate, *International Journal of Heat and Mass Transfer*, *106* (2017), Mar., pp. 989-996
[21] Yang, L. L., *et al*., The Fabrication of Micro/Nanostructures by Laser Machining, *Nanomaterials*, *9* (2019), 12, 1789
[22] Alvarez, F. X., Jou, D., Size and Frequency Dependence of Effective Thermal Conductivity in Nanosystems, *Journal of Applied Physics*, *103* (2008), 9, 094321
[23] Al-Nimr, M. A., Kiwan, S., Effect of Thermal Losses on the Microscopic Two-Step Heat Conduction Model, *International Journal of Heat and Mass Transfer*, *44* (2001), 5, pp. 1013-1018
[24] Alvarez, F. X., Jou, D., Memory and Non-Local Effects in Heat Transport: From Diffusive to Ballistic Reegimes, *Applied Physics Letters*, *90* (2007), 8, 083109
[25] Alvarez, F. X., Jou, D., Boundary Conditions and Evolution of Ballistic Heat Transport, *ASME Journal of Heat Transfer*, *132* (2010), 012404
[26] Mao, Y. D., Xu, M. T., Non-Fourier Heat Conduction in a Thin Gold Film Heated by an Ultra-Fast-Laser, *Science China (Technological Sciences)*, *58* (2015), 04, pp. 638-649

[27] Cheng, L., *et al*., Single- and Dual-Phase-Lagging Heat Conduction Models in Moving Media, *ASME Journal of Heat Transfer*, *130* (2008), 12, pp. 1-6
[28] Choudhuri, S. R., On a Thermoelastic Three-Phase-Lag Model, *Journal of Thermal Stresses*, *30* (2007), July, pp. 231-238
[29] Mondal, S., *et al*., Fractional Order Two-Temperature Dual-Phase-Lag Thermoelasticity with Variable Thermal Conductivity, *International Scholarly Research Notices*, *2014* (2014), 3, 646049
[30] Mao, Y. D., Xu, M. T., Lattice Boltzmann Numerical Analysis of Heat Transfer in Nanoscale Silicon Films Induced by Ultra-Fast Laser Heating, *International Journal of Thermal Sciences*, *89* (2015), Mar., pp. 210-221

Paper submitted: August 19, 2022
Paper revised: December 28, 2022
Paper accepted: January 13, 2023